



CHORUS

This is the accepted manuscript made available via CHORUS. The article has been published as:

Local Jahn-Teller distortions and orbital ordering in $\text{Ba}_3\text{Cu}_{1+x}\text{Sb}_{2-x}\text{O}_9$ investigated by neutron scattering

Bing Li, Despina Louca, Mikhail Feygenson, Craig M. Brown, John R. D. Copley, and Kazuki Iida

Phys. Rev. B **93**, 014423 — Published 15 January 2016

DOI: [10.1103/PhysRevB.93.014423](https://doi.org/10.1103/PhysRevB.93.014423)

Local Jahn-Teller distortions and orbital ordering in $\text{Ba}_3\text{Cu}_{1+x}\text{Sb}_{2-x}\text{O}_9$ investigated by neutron scattering

Bing Li,¹ Despina Louca,^{1,*} Mikhail Feygenson,² Craig M. Brown,³ John R. D. Copley,³ and Kazuki Iida⁴

¹*Department of Physics, University of Virginia, Charlottesville, VA 22904*

²*Spallation Neutron Source, Oak Ridge National Laboratory, Oak Ridge, TN 37831*

³*Center for Neutron Research, National Institute of Standards and Technology, Gaithersburg, MD 20899*

⁴*Research Center for Neutron Science and Technology, Tokai, Ibaraki 319-1106, Japan.*

(Dated: December 29, 2015)

A spin-orbital quantum liquid state is theoretically proposed in the honeycomb lattice of $\text{Ba}_3\text{CuSb}_2\text{O}_9$, enabled by dynamic short-range correlations between the spin and orbital degrees of freedom. Using neutron diffraction, the local atomic structure of $\text{Ba}_3\text{Cu}_{1+x}\text{Sb}_{2-x}\text{O}_9$ at $x = 0$ and 0.1 is obtained via the pair density function analysis. The results indicate that both compositions exhibit local Jahn-Teller (JT) distortions with the elongated CuO_3 octahedral configuration. In $\text{Ba}_3\text{Cu}_{1.1}\text{Sb}_{1.9}\text{O}_9$, JT ordering of the distorted CuO_3 octahedra gives rise to the orthorhombic symmetry with ferro-orbital order. On the other hand, in $\text{Ba}_3\text{CuSb}_2\text{O}_9$, even though the CuO_3 octahedra are JT distorted, there is no long-range ordering hence the symmetry is hexagonal. Furthermore, the local singlet excitation at 5.8 meV observed in $\text{Ba}_3\text{CuSb}_2\text{O}_9$ below 50 K is absent in $\text{Ba}_3\text{Cu}_{1.1}\text{Sb}_{1.9}\text{O}_9$. Instead, an excitation at 2.5 meV is observed in the latter, that is likely associated with short-range spin order.

PACS numbers: 61.05.F-, 61.66.Fn, 75.20.-g

I. INTRODUCTION

A quantum spin liquid is a state of matter dominated by quantum fluctuations that prevent long-range spin order even at the lowest temperature, in spite of strong interactions¹⁻³. The experimental realization of a quantum spin liquid state in real materials has been a central issue in condensed matter physics. Magnetic systems where antiferromagnetically coupled magnetic ions reside on triangular or tetrahedral motifs are often rendered susceptible to magnetic frustration, which results in fluctuations⁴⁻¹². Several materials have been suggested as possible candidates in which a quantum spin liquid state can be realized such as in the Cu^{2+} based triangle-lattice organic salts and in the kagome lattice of $\text{ZnCu}_3(\text{OH})_6\text{Cl}_2$ ^{13,14}.

Recently, a new system has been reported as a possible candidate for exhibiting a spin liquid state, $\text{Ba}_3\text{CuSb}_2\text{O}_9$, with spin-1/2 Cu^{2+} ions¹⁵. $\text{Ba}_3\text{CuSb}_2\text{O}_9$ crystallizes in the centrosymmetric hexagonal $P6_3/mmc$ structure, where the Cu and Sb ions are in octahedral environments as shown in Fig. 1(a). Sandwiched between the Sb1 oxygen coordinated octahedra are the Sb2/Cu shared octahedra shown in blue. Based on the 2:1 ratio of Sb to Cu, these octahedra are equally shared in the average symmetry by Cu and Sb2 ions introducing site disorder¹⁶. The centrosymmetric structure shown in Fig. 1(a) is different from the non-centrosymmetric hexagonal $P6_3mc$ structure suggested from earlier works¹⁷. This is shown in Fig. 1(b) for comparison. The most distinct difference between the two symmetries is the absence of Cu/Sb2 shared octahedral site in the latter symmetry i.e. the Cu octahedra are highlighted in pink while the Sb2 octahedra are in brown just like the Sb1 octahedra. It is due to this site disorder that the centrosymmetry

is retained in $P6_3/mmc$, but clearly absent in $P6_3mc$. A number of experiments including magnetic susceptibility, neutron diffraction, μSR and NMR have indicated that there is no magnetic order down to 20 mK, even though the Curie-Weiss temperature is estimated to be $\theta_{CW} \sim -55$ K^{15,16,18}. Separately, a cooperative Jahn-Teller (JT) effect of the Cu^{2+} ion, presumably absent in the spin liquid state of $\text{Ba}_3\text{CuSb}_2\text{O}_9$, was found in non-stoichiometric compounds in which the copper concentration is increased from one as in $\text{Ba}_3\text{Cu}_{1+x}\text{Sb}_{2-x}\text{O}_9$ and the symmetry is lowered from the hexagonal to an orthorhombic structure with the $Cmcm$ symmetry with the transition occurring at about 200 K^{16,19}. The orthorhombic structure is shown in Fig. 1(c). In this symmetry, the Cu and Sb2 octahedra are also shared as seen in the blue octahedra.

Theoretical and experimental works have pointed out that the spin and orbital degrees of freedom might be strongly entangled, possibly enabling a spin-orbital liquid state in $\text{Ba}_3\text{CuSb}_2\text{O}_9$ ^{16,20-25}. In this paper, we compare the local atomic structures of $\text{Ba}_3\text{Cu}_{1+x}\text{Sb}_{2-x}\text{O}_9$ with $x = 0$ and 0.1. We find that locally the Cu^{2+} ions are JT distorted in both compositions but the CuO_3 octahedra are not ordered in the same way. In the $x = 0.1$, the ferro-orbital model in which the JT-distorted octahedra align in the bc-plane fits the data quite well, but the same model cannot fit the data of the $x = 0$ composition as well implying a more complex orbital arrangement.

II. EXPERIMENT

The powder samples of $\text{Ba}_3\text{Cu}_{1+x}\text{Sb}_{2-x}\text{O}_9$ ($x = 0$ and 0.1) were prepared by conventional solid state reaction method following the procedure described in Ref.¹⁵.

The $x = 0$ is referred to as Cu1.0 and the $x = 0.1$ as Cu1.1 in the figures. The neutron scattering measurements were performed as a function of temperature at the Nanoscale Ordered Materials Diffractometer (NOMAD) at the Spallation Neutron Source of Oak Ridge National Laboratory²⁶ and at the BT-1 powder diffractometer, at the NIST Center for Neutron Research, using a Ge (733) monochromator with a constant wavelength of 1.1969 Å. The diffraction data from BT-1 were analyzed by the Rietveld refinement method to obtain the average structure. The NOMAD data were corrected for instrumental background and sample containment, and normalized by a vanadium standard. Separately, absorption and multiple scattering corrections were applied as well. The structure function, $S(Q)$, obtained from the diffraction data as a function of Q , the momentum transfer, was Fourier transformed to obtain the pair density function, $G(r)$, using a termination Q_{max} of 40 Å⁻¹. This analysis provides the local arrangement of atoms and is very sensitive to short-range distortions. This technique is analogous to the EXAFS technique, although it provides reliable information beyond first nearest neighbors. Further details can be found in Refs.^{27,28}. The $G(r)$ consists of correlation peaks that correspond to the probability of finding a particular pair of atoms at a given distance in space.

$$G(r) = \frac{2}{\pi} \int_0^{Q_{max}} Q(S(Q) - 1) \sin(Qr) dQ, \quad (1)$$

The inelastic neutron scattering experiment was performed on powder samples with masses around 30 grams, at the disk chopper spectrometer (DCS) at the NIST Center for Neutron Research, with a wavelength of 2.5 Å. From this data, the dynamic structure factor, $S(Q, E)$, can be obtained.

III. RESULTS AND DISCUSSION

A. Crystal structure

The diffraction data collected on the Ba₃CuSb₂O₉ sample on NOMAD were analyzed using the $P6_3/mmc$ and $P6_3mc$ symmetries. Shown in Fig. 2 (a) is the diffractogram at 10 K compared to the two models determined from these symmetries. The fits are almost identical and no differences can be discerned from the neutron measurements on NOMAD between the two. Given that the $P6_3/mmc$ is a higher symmetry, we refined the remaining temperatures using this symmetry. The temperature dependence of the lattice constants a and c are shown in Figs. 2(b) and 2(c). The replacement of Sb⁵⁺ ions with 10 % of Cu²⁺ ions has been proposed to lead to a structural phase transition to the $Cmcm$ symmetry¹⁶. The diffraction data collected on NOMAD on the Ba₃Cu_{1.1}Sb_{1.9}O₉ at 10 K was refined using both $Cmcm$ and $P6_3/mmc$ symmetries as well, only

to find out that no discernible differences can be observed between the two either. The excess Cu leads to an increase in both the a and c -lattice constants due to the nominally bigger size of Cu²⁺ compared with Sb⁵⁺ (²⁹), giving rise to a smaller a/c ratio. Another element that is different between Ba₃CuSb₂O₉ and Ba₃Cu_{1.1}Sb₂O₉ is the isotropic Debye-Waller factor (U_{iso}) of the Cu/Sb2 site. The U_{iso} of Cu/Sb2 in Ba₃CuSb₂O₉ is larger than that in Ba₃Cu_{1.1}Sb_{1.9}O₉. The diffraction data collected on BT-1 at the NCNR on the $x = 0.1$ sample at 10 and 300 K are compared in the region of the (300) Bragg peak, with momentum transfer, Q , around $Q = 3.75$ Å⁻¹. Although the pattern shifts due to the expansion of the lattice with increasing temperature, there are no discernible structural differences between them. Thus within the resolution of the BT-1 diffractometer we cannot observe the structural phase transition to $Cmcm$ proposed earlier. The refined occupancy of Cu is 0.5617 while that of Sb2 is 0.4383, close to the nominal composition. A split of the (300) peak is expected when the orthorhombic distortion arises, as observed in the synchrotron X-ray diffraction measurement reported in Ref.¹⁶. The split is clearly absent in the neutron diffraction data because the neutron structure function is quite weak at the particular point in Q .

B. Local structure

Ba₃CuSb₂O₉ : We now turn our attention to the local structure. The PDF, $G(r)$, corresponding to the local structure of Ba₃CuSb₂O₉, determined from the data collected at 2 K is shown in Fig. 3(a). The data is compared to a model calculated using as input the atomic coordinates and unit cell dimensions of the hexagonal $P6_3/mmc$ unit cell. In the $P6_3/mmc$ symmetry, the Cu²⁺ and Sb⁵⁺ ions share a site creating a regular triangular lattice. The first peak in the data corresponds to Cu-O and Sb-O octahedral pair correlations with a small shoulder to the right that is not reproduced in the model PDF constructed from the $P6_3/mmc$ structure. Instead, the first peak in the model is symmetric. Additional differences between the model and data are observed at greater distances as well as shown in the inset, around 6 Å, corresponding to correlations between next nearest neighbor Cu/Sb2-Cu/Sb2 pairs. Thus locally, the symmetry is lower than the hexagonal $P6_3/mmc$.

How are the Cu and Sb2 ions spatially arranged? To determine their local environment, the 2 K data of Ba₃CuSb₂O₉ is compared to a second model calculated using the atomic coordinates and unit cell dimensions of the $Cmcm$ symmetry even though this symmetry is not used to fit the data on average. The fitting to the local structure is shown in Fig. 3(b). In the $Cmcm$ symmetry, the Cu²⁺ and Sb⁵⁺ ions also share a site and yield a very similar local arrangement as in the $P6_3/mmc$ crystal model. However, in the orthorhombic symmetry, the b -axis is doubled due to JT ordering of the octahedra,

and the Cu-O bonds are split to 4 short and 2 long, with lengths at 2.01 and 2.12 Å that can explain the shoulder to the right of the first peak in the experimental data. However, due to Cu/Sb2 site disorder and the significant overlap of Cu-O and Sb1/2-O bonds, the bond length differences are not sufficient to visibly reproduce the shoulder.

A third model is calculated based on the atomic coordinates of the non-centrosymmetric $P6_3mc$ symmetry and shown in Fig. 3(c). In this case, the Cu^{2+} and Sb^{5+} ions are split as shown in the inset and also in Fig. 1(b). The Cu^{2+} ions are at the $2b$ Wyckoff site coordinated by six O^{2-} ions with three long and three short bonds, an arrangement that is not compatible with the JT distortion of the Cu^{2+} in the octahedral configuration. The Cu^{2+} ions form a triangle lattice layer in the ab plane, separated by two nonmagnetic $\text{Sb}_2\text{O}_{9/2}$ face-sharing layers. As it can be seen from Fig. 3(c), the first peak is not reproduced well by this model because it yields a symmetric peak just as in the $P6_3/mmc$ symmetry. The fitting at longer distances however is improved compared to both the $P6_3/mmc$ and $Cmcm$ models. In particular, the structure in the data PDF around 6 Å is reproduced well while small differences are observed in the relative intensities between the peaks. The differences between $P6_3mc$ and the two previously discussed symmetries, $P6_3/mmc$ and $Cmcm$, arise from the absence of site-disorder of the Cu and Sb2 ions in $P6_3mc$. This indicates that Cu and Sb2 most likely do not share a site and may be locally ordered.

The local arrangement of Cu and Sb2 is explored further by considering the superposition of two hypothetical compounds: one is "Ba₃Sb₃O₉" with regular $\text{SbO}_{6/2}$ octahedra and uniform Sb-O bonds at 2.0 Å and the second is "Ba₃Cu₃O₉" with cooperative JT distortion giving rise to a two long (2.20 Å) and four short (2.0 Å) bond configuration. In Fig. 4, the data for Ba₃CuSb₂O₉ in the region encompassing the first peak is compared between the two models. When the two hypothetical models are added at a ratio of one to two, the superposition yields a model that fits the experimental data quite well (green line), strongly indicating that in Ba₃CuSb₂O₉, the Cu^{2+} octahedra are most likely JT distorted. Given that only 1/3 of the octahedral sites consist of Cu, the number of long bonds is 1/9 of the total number hence the intensity of the peak is weak. Nonetheless, it is clear that the Cu octahedra are JT distorted and this distortions needs to be included in the local model. Which model can reproduce this environment?

The fitting of the local structure and in particular of the first peak corresponding to the JT distorted Cu octahedra significantly improves when using an earlier proposed ferro-orbital model²⁰ in the coordinate frame of the $Cmcm$ symmetry. In this model, the JT octahedra are aligned in one direction and the Cu and Sb2 ions are ordered in the honeycomb pattern shown in Fig. 5(a). The Cu hexagon has an Sb octahedron in the center. This octahedral configuration is consistent with a den-

sity functional theory (DFT) calculation that yielded a single occupancy of the $3d_{x^2-y^2}$ orbital³⁰. Below the Cu hexagon, the face-sharing Sb2 octahedra make the same honeycomb ring with a Cu octahedron in the center. In the ferro-orbital model, the Cu octahedra are elongated and are uniformly aligned in the bc -plane with no distortion along the a axis. As a result, two sets of Cu-Cu distances are created, at 5.69 and 5.82 Å, as shown in the figure.

The comparison of the ferro-orbital model with the local structure of Ba₃CuSb₂O₉ is shown in Fig. 5(b). This model fits the data fairly well as seen in the figure, especially at the shoulder of the first PDF peak and shows further improvement in the region around 6 Å. This can be seen by comparing all panels of Fig. 3 and Fig. 5(b). The ferro-orbital model is used to fit the data at higher temperatures as well. With increasing temperature, the PDF peaks become broader due to thermal vibrations and the features at 2.2 and 6 Å become less discernible. However, they are still visible at 300 K. The JT distortion of the Cu octahedra is extremely stable and usually persists up to the melting point, as was found in other cuprates³¹. Thus it is clear that the Cu octahedra are JT distorted in Ba₃CuSb₂O₉.

Ba₃Cu_{1.1}Sb_{1.9}O₉: The same ferro-orbital model used in modeling the local structure of Ba₃CuSb₂O₉ can reproduce the experimental data of the Ba₃Cu_{1.1}Sb_{1.9}O₉ as well. Given that the average symmetry of the Cu1.1 is orthorhombic, the ferro-orbital model is based on this symmetry. The JT distortion is evident in the first peak in Cu1.1 just as in the Cu1.0, while the local structure at longer distances fits better, giving rise to a lower agreement factor, with some small differences observed between the model and data around 5.5 Å as shown in the right inset in Fig. 5(c). The comparison of the fitting of the Cu1.0 data to the fitting of the Cu1.1 leads us to conclude that the ferro-orbital model fits the data of the Cu1.1 quite well and does a better job in fitting the data of the Cu1.0 in comparison to all the existing models plotted in Fig. 3. It is possible that while the JT Cu octahedra and Cu-Sb2 ordering are present in both samples, the exact nature of the orbital tilting and local ordering are most likely different in the two compositions. A recent X-ray Huang scattering experiment suggested that ferro- and antiferro-orbital correlations are competing in Ba₃CuSb₂O₉²⁰ that may be the case here as well as ferro- and antiferro-orbital states cannot be distinguished if they involve the same bond lengths.

C. Inelastic data

The dynamic structure factor, $S(Q, E)$, is obtained from the inelastic data collected on DCS. Shown in Fig. 6 is the $S(Q, E)$ integrated in the Q region between 0.8 and 2.0 Å⁻¹ where the magnetic signal is expected to have a significant contribution. The data are plotted at different temperatures in the energy range of 4 to 7.5

meV. The symbols correspond to data points while the solid lines are Gaussian fits to the data. In $\text{Ba}_3\text{CuSb}_2\text{O}_9$, a broad excitation is observed at 1.5 K, centered around 5.8 meV, as shown in Fig. 6(a). With increasing temperature, it becomes even broader and finally disappears between 50 and 100 K (see 6(b) and 6(c)). This data is consistent with previous reports¹⁶. The excitation around 5.8 meV has been attributed to be due to a local singlet arising from the antiferromagnetic coupling between Cu^{2+} spins. However, such an excitation is not observed in $\text{Ba}_3\text{Cu}_{1.1}\text{Sb}_{1.9}\text{O}_9$ as seen in Fig. 6(d), which suggests that the singlet state is suppressed by the 10 % substitution of Cu for Sb.

Instead, a more striking feature in our data is the presence of a new excitation observed at 2.5 meV in $\text{Ba}_3\text{Cu}_{1.1}\text{Sb}_{1.9}\text{O}_9$ at 1.5 K. In Fig. 6(e), the lower energy portion of the $S(Q, E)$ is shown. After subtracting the elastic line (red line), a well-defined peak centered at 2.5 meV remains, that is fit well by a Gaussian function (blue line). This is clearly absent in $\text{Ba}_3\text{CuSb}_2\text{O}_9$, where the spectrum is well described by the elastic line as shown in Fig. 6(f). The peak is broad in energy that suggests the excitations may be local in nature. The substitution of Cu for Sb most likely leads to a dilute triangle lattice of Cu^{2+} . In the stoichiometric $\text{Cu}_{1.0}$ the Cu ions are arranged in a hexagon. When more Cu is added to replace Sb, the symmetry will be broken and a triangle lattice will be created in regions where Cu is in excess but not everywhere. This can give rise to a dilute triangle lattice of Cu which suppresses the spin singlet state observed in $\text{Ba}_3\text{CuSb}_2\text{O}_9$. On the other hand, in a triangle lattice Heisenberg antiferromagnet, long-range order is expected as in a related system, the $\text{Ba}_3\text{CoSb}_2\text{O}_9$ ³². The coupling constant, J/k_B , has been estimated for a triangle lattice of Cu^{2+} in $\text{Ba}_3\text{CuSb}_2\text{O}_9$ to be 32 K (from a high-temperature series expansion) and 37 K (from mean-field theory)¹⁵. Thus it is possible that $\text{Ba}_3\text{Cu}_{1.1}\text{Sb}_{1.9}\text{O}_9$ can be seen as a dilute triangle lattice Heisenberg antiferromagnet and the excitation at 2.5 meV is most likely related to local freezing of spins.

The powder averaged $S(Q, E)$ function was calculated for an isolated $S=1/2$ spin dimer model with an interatomic distance of 5.7879 Å that corresponds to the spacing of Cu sites in $\text{Ba}_3\text{Cu}_{1.1}\text{Sb}_2\text{O}_9$. When $J = 29$ K, the resulting $S(Q, E)$ integrated in the Q-range from 0.8 to 2 Å⁻¹ can fit the experimental data at 1.5 K quite well, as shown in Fig. 7(a). At lower Q, this model is also able to reproduce the data as seen in Fig. 7(b), while an apparent deviation is observed when Q increases to values larger than 2 Å⁻¹, most likely due to phonons. This isolated dimer model is highly possible given that the stoichiometric $\text{Ba}_3\text{CuSb}_2\text{O}_9$ is proposed to be a correlated spin dimer system.

D. Discussion

The JT effect is dominant in the $\text{Ba}_3\text{Cu}_{1+x}\text{Sb}_{2-x}\text{O}_9$ system. In the case of strong spin-orbital coupling, the presence of a cooperative JT ordering will most likely lead to spin ordering. In both compounds, local JT ordering is possible. On the honeycomb lattice, two adjacent octahedra distort in the same direction and the two spins on these sites form a singlet. If the distortion is randomized in every direction i.e. the overall distortion is canceled when the octahedra are tilted in different directions, the hexagonal symmetry will appear on average. Thus long-range cooperative ordering is less likely due to the lattice strain. This is what is observed in $\text{Ba}_3\text{CuSb}_2\text{O}_9$. In the other hand, the substitution of Sb by Cu breaks the symmetry and induces a transition to the orthorhombic phase, albeit very weak, with a long-range orbital order. This configuration favors spin freezing, just as observed in off-stoichiometric compositions at 100 mK¹⁶.

It has been proposed theoretically that when a spin-orbital resonance is facilitated by a dynamic JT effect, a spin-orbital liquid may appear where spin-orbital correlations play a critical role²¹. From the X-ray Huang scattering measurement²⁰, it was proposed that the ferro-orbital interactions are saturated at 50 K while antiferro-orbital correlations appear to dominate at lower temperatures. At the same time, NMR measurement pointed out that a local spin singlet is formed at this temperature. From our local structure and inelastic neutron scattering studies on the two samples, we observed that $\text{Ba}_3\text{CuSb}_2\text{O}_9$ and $\text{Ba}_3\text{Cu}_{1.1}\text{Sb}_{1.9}\text{O}_9$ have different spin and orbital states. In $\text{Ba}_3\text{CuSb}_2\text{O}_9$, there is an excitation at 5.8 meV associated with the spin singlet that sets in around 50 K. The PDF analysis suggests that the orbital state cannot be completely reproduced by ferro-orbital ordering. In contrast, the ferro-orbital model can describe the data of $\text{Ba}_3\text{Cu}_{1.1}\text{Sb}_{1.9}\text{O}_9$ better. However, the excitation at 5.8 meV is not observed in the latter compound while a new excitation appears at 2.5 meV, that might be related to local spin freezing due to the partial triangle lattice of Cu^{2+} originating from the 10 % substitution at the Sb site.

To summarize, in order to examine the local ionic order, we have systematically studied $\text{Ba}_3\text{Cu}_{1+x}\text{Sb}_{2-x}\text{O}_9$ ($x = 0$ and 0.1) by powder neutron diffraction and the PDF analysis. Focusing on the local atomic structure around 6 Å that corresponds to contributions from Cu-Sb2 bond correlations, we find that the Cu and Sb2 ions are locally ordered in both compounds by comparing three different local structural models. Moreover, the Cu^{2+} is locally JT active, which is consistent with the EXAFs results and DFT calculations. At the same time, some local differences are observed between the two systems that indicate the their orbital ordering is most likely different. The ferro-orbital model describes the local structure of $\text{Ba}_3\text{Cu}_{1.1}\text{Sb}_{1.9}\text{O}_9$ very well, in which the elongated $\text{CuO}_{6/2}$ octahedra align in a unique direction on a distorted honeycomb lattice with Cu-Sb2 ordering.

This arrangement leads to a $3d_{x^2-y^2}$ orbital order. This model does not fit the data for $\text{Ba}_3\text{CuSb}_2\text{O}_9$ however, even though the JT distortion and Cu-Sb2 broken site symmetry can be reproduced. $\text{Ba}_3\text{CuSb}_2\text{O}_9$ may have a more complex local structure. Furthermore, the low energy spin excitations exhibit very different behaviors in the two systems: in $\text{Ba}_3\text{CuSb}_2\text{O}_9$ a spin singlet excitation at 5.8 meV is observed while in $\text{Ba}_3\text{Cu}_{1.1}\text{Sb}_{1.9}\text{O}_9$

the spin singlet excitation is absent but a separate broad excitation at 2.5 meV is observed instead.

This work has been supported by the Department of Energy, Grant number DE-FG02-01ER45927. We acknowledge the support of the National Institute of Standards and Technology, U. S. Department of Commerce, in providing the neutron research facilities used in this work.

-
- * Electronic address: louca@virginia.edu
- ¹ *Introduction to Frustrated Magnetism: Materials, Experiments, Theory*, edited by C. Lacroix, P. Mendels, and F. Mila (Springer Series in Solid-State Sciences, Vol. **164**) (2011).
 - ² L. Balents, *Nature (London)* **464**, 199 (2010).
 - ³ P. W. Anderson, *Mater. Res. Bull.* **8**, 153 (1973).
 - ⁴ M. J. Harris, S. T. Bramwell, D. F. McMorrow, T. Zeiske, and K. W. Godfrey, *Phys. Rev. Lett.* **79**, 2554 (1997).
 - ⁵ I. Mirebeau and I. N. Goncharenko, *J. Phys. Condens. Matter* **17**, S771 (2005).
 - ⁶ P. W. Anderson, *Phys. Rev.* **102**, 1008 (1956).
 - ⁷ A. P. Ramirez, *Ann. Rev. Mater. Sci.* **24**, 453 (1994).
 - ⁸ J. A. Mydosh, in *Spin Glasses, an Experimental Introduction* (Taylor and Frances, London, 1993).
 - ⁹ Z. Zhang, Despina Louca, A. Visinoiu, S.-H. Lee, J. D. Thompson, Y. Qiu, T. Proffen, A. Llobet, and S. Park, *Phys. Rev. B* **74**, 014108 (2006).
 - ¹⁰ T. Yoshioka, A. Koga, and N. Kawakami, *J. Phys. Soc. Jpn.* **73**, 1805 (2004).
 - ¹¹ T. Yildirim, A. B. Harris and E. F. Shender, *Phys. Rev. B* **58**, 3144 (1998).
 - ¹² S.-H. Lee, C. Broholm, W. Ratcliff, G. Gasparovic, Q. Huang, T. H. Kim, and S. W. Cheong, *Nature (London)* **418**, 856 (2002).
 - ¹³ S. Yamashita, Y. Nakazawa, M. Oguni, Y. Oshima, H. Nojiri, Y. Shimizu, K. Miyagawa, and K. Kanoda, *Nat. Phys.* **4**, 459 (2008).
 - ¹⁴ T.-H. Han, J. S. Helton, S. Chu, D. G. Nocera, J. A. Rodriguez-Rivera, C. Broholm, and Y. S. Lee, *Nature (London)* **492**, 406 (2012).
 - ¹⁵ H. D. Zhou, E. S. Choi, G. Li, L. Balicas, C. R. Wiebe, Y. Qiu, J. R. D. Copley, and J. S. Gardner, *Phys. Rev. Lett.* **106**, 147204 (2011).
 - ¹⁶ S. Nakatsuji et al., *Science* **336**, 559 (2012).
 - ¹⁷ Von. P. Köhlet al., *Z. Anorg. Allg. Chem.* **442**, 280 (1978).
 - ¹⁸ J. A. Quilliam, F. Bert, E. Kermarrec, C. Payen, C. Guillot-Deudon, P. Bonville, C. Baines, H. Luetkens, and P. Mendels, *Phys. Rev. Lett.* **109**, 117203 (2012).
 - ¹⁹ N. Katayama, K. Kimura, Y. Han, J. Nasu, N. Drichko, Y. Nakanishi, M. Halim, Y. Ishiguro, R. Satake, E. Nishibori, M. Yoshizawa, T. Nakano, Y. Nozue, Y. Wakabayashi, S. Ishihara, M. Hagiwara, H. Sawa, S. Nakatsuji, *Proc. Natl. Acad. Sci. U.S.A.* **112**, 9305 (2015).
 - ²⁰ Y. Ishiguro, K. Kimura, S. Nakatsuji, S. Tsutsui, A. Baron, T. Kimura, and Y. Wakabayashi, *Nat. Commun.* **4**, 2022 (2013).
 - ²¹ J. Nasu and S. Ishihara, *Phys. Rev. B* **88**, 094408 (2013).
 - ²² A Smerald and F. Mila, *Phys. Rev. B* **90**, 094422 (2014).
 - ²³ P. Corboz, M. Lajkó, A. M. Läuchli, K. Penc, and F. Mila, *Phys. Rev. X* **2**, 041013 (2012).
 - ²⁴ A. Smerald and F. Mila, *Phys. Rev. Lett.* **115**, 147202 (2015).
 - ²⁵ S.-H. Do, J. van Tol, H. D. Zhou, and K.-Y. Choi, *Phys. Rev. B* **90**, 104426 (2014).
 - ²⁶ J. Neuefeind, M. Feyngenson, J. Carruth, R. Hoffmann, K. Chingley, *Nucl. Instrum. Meth. B* **287**, 68 (2012).
 - ²⁷ D. Louca, T. Egami, E. L. Brosha, H. Röder and A. R. Bishop, *Phys. Rev. B* **56**, R8475 (1997).
 - ²⁸ T. Egami, Y. Petrov and D. Louca, *J. Superconductivity* **13**, 709 (2000).
 - ²⁹ R. D. Shannon, *Acta Cryst.* **A32**, 751 (1976).
 - ³⁰ K. V. Shanavas, Z. S. Popović, and S. Satpathy, *Phys. Rev. B* **89**, 085130 (2014).
 - ³¹ H. Tanaka, H. Dachs, K. Iio, and K. Nagata, *J. Phys. C* **19**, 4861 (1986).
 - ³² Y. Doi, Y. Hinatsu, and K. Ohoyama, *J. Phys. Condens. Matter* **16**, 8923 (2004).

Figure captions:

Figure 1: The crystal structure of $\text{Ba}_3\text{Cu}_{1+x}\text{Sb}_{2-x}\text{O}_9$ is shown using three different symmetries: (a) $P6_3/mmc$, (b) $P6_3mc$ and (c) $Cmcm$. Only the Cu and Sb octahedra are shown.

Figure 2: (a) The neutron diffraction intensity from data collected on NOMAD for $\text{Ba}_3\text{CuSb}_2\text{O}_9$ is compared to two models with $P6_3/mmc$ and $P6_3mc$ symmetries at 10 K. Shown in (b) and (c) is the temperature dependence of the lattice constants of $\text{Ba}_3\text{CuSb}_2\text{O}_9$ and $\text{Ba}_3\text{Cu}_{1.1}\text{Sb}_{1.9}\text{O}_9$ determined by the refinement of the NOMAD data.

Figure 3: The comparisons of the experimental PDFs with different models at 2 K for $\text{Ba}_3\text{CuSb}_2\text{O}_9$: (a) $P6_3/mmc$, (b) $Cmcm$, (c) $P6_3mc$. The insets highlight the features around 6 Å. The right panels show the corresponding arrangement of Cu and Sb ions. The difference between (a) and (b) is that the triangle lattice in $Cmcm$ is distorted.

Figure 4: A comparison of the experimental data of $\text{Ba}_3\text{CuSb}_2\text{O}_9$ at 2 K with two hypothetical models corresponding to "Ba₃Sb₃O₉", "Ba₃Cu₃O₉", and their superposition.

Figure 5: (a) The local ferro-orbital model based on the Cu^{2+} and Sb^{5+} dumbbell order. The JT distortion of the $\text{CuO}_{6/2}$ octahedron with the four short (2.00 Å)

and two long (2.20 Å) configuration is indicated in the figure. The right panel is the corresponding $x^2 - y^2$ orbital state. The hexagon is not perfect due to the JT effect. The comparison of the experimental PDF with the ferro-orbital model at 2 K for $\text{Ba}_3\text{CuSb}_2\text{O}_9$ is shown in (b) and for $\text{Ba}_3\text{Cu}_{1.1}\text{Sb}_{1.9}\text{O}_9$ is shown in (c). The insets highlight the features around 4.5 and 6 Å.

Figure 6: The $S(Q, E)$ is integrated in Q from 0.8 to 2 Å⁻¹ and plotted around the energy region of 6 meV. In (a), the data is shown for $\text{Ba}_3\text{CuSb}_2\text{O}_9$ at 1.5 K, at 50 K in (b) and at 100 K in (c). In (d), the data is shown for $\text{Ba}_3\text{Cu}_{1.1}\text{Sb}_{1.9}\text{O}_9$ at 1.5 K. In (e), the lower energy part around 3 meV is shown for $\text{Ba}_3\text{Cu}_{1.1}\text{Sb}_{1.9}\text{O}_9$ at 1.5 K, and in (f), the data is shown for $\text{Ba}_3\text{CuSb}_2\text{O}_9$ at 1.5 K. The symbols are data points while the solid lines are the Gaussian function fitting. In (e), the dynamic structure factor in solid symbols is obtained by subtracting the elastic line, which fits well to a Gaussian function centered at 2.5 meV.

Figure 7: The fit of the inelastic intensity with an isolated spin dimer model of S-1/2 with spacing $d = 5.7879$ Å and exchange interaction $J = 29$ K. (a) The energy dependence of the $S(Q, E)$ integrated in Q from 0.8 to 2 Å⁻¹. The inset schematically shows the spin dimer. (b) The Q dependence of the $S(Q, E)$ integrated in energy, E , from 2 to 3 meV.

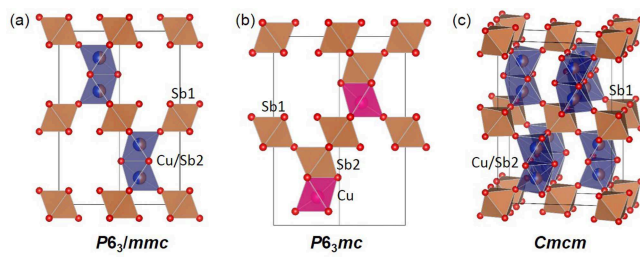


Figure 1

29Dec2015

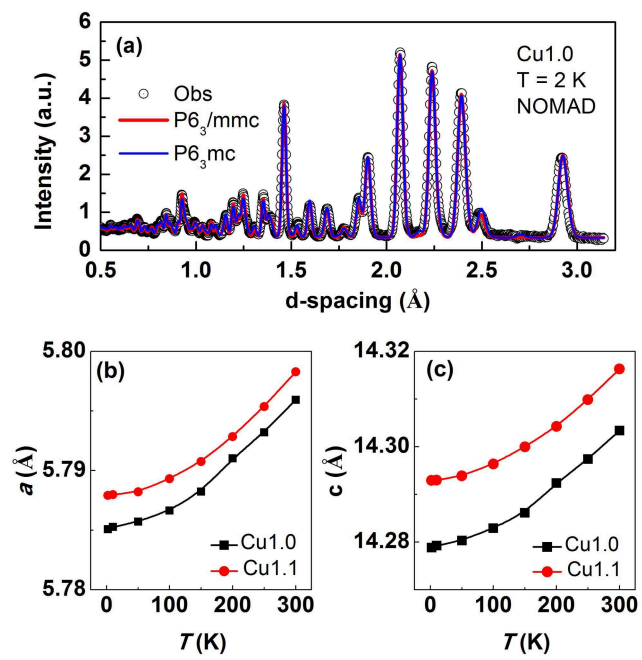


Figure 2

29Dec2015

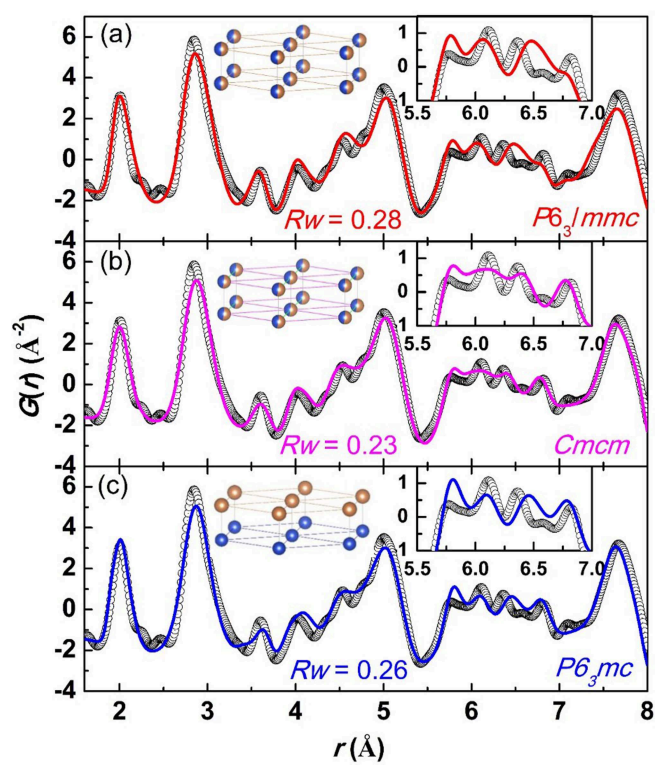


Figure 3

29Dec2015

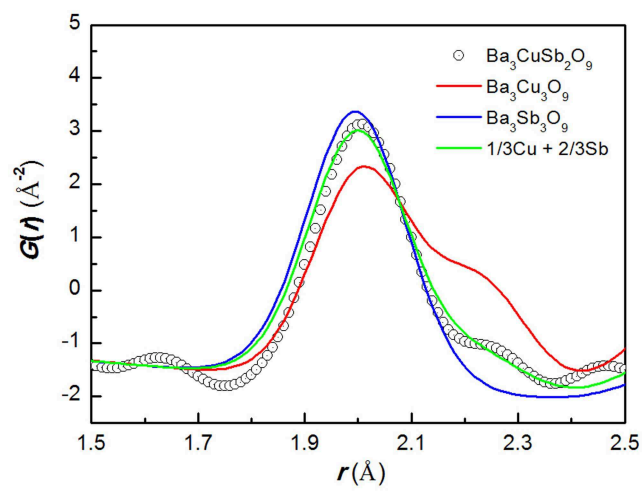


Figure 4

29Dec2015

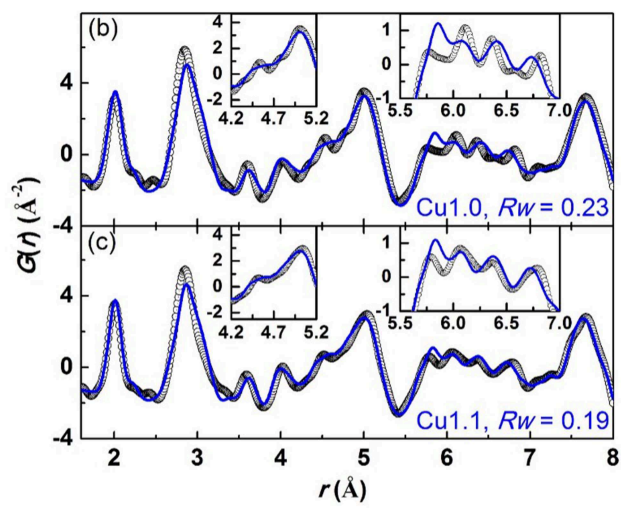
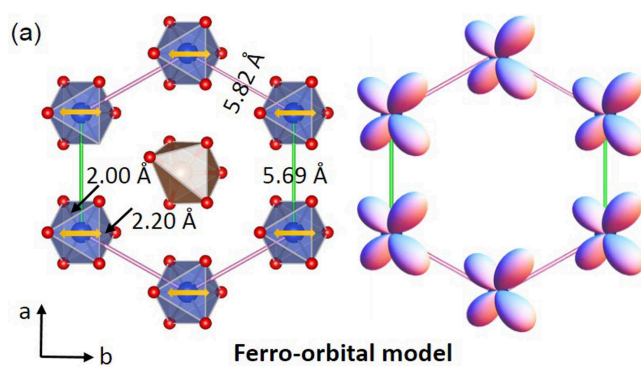


Figure 5

29Dec2015

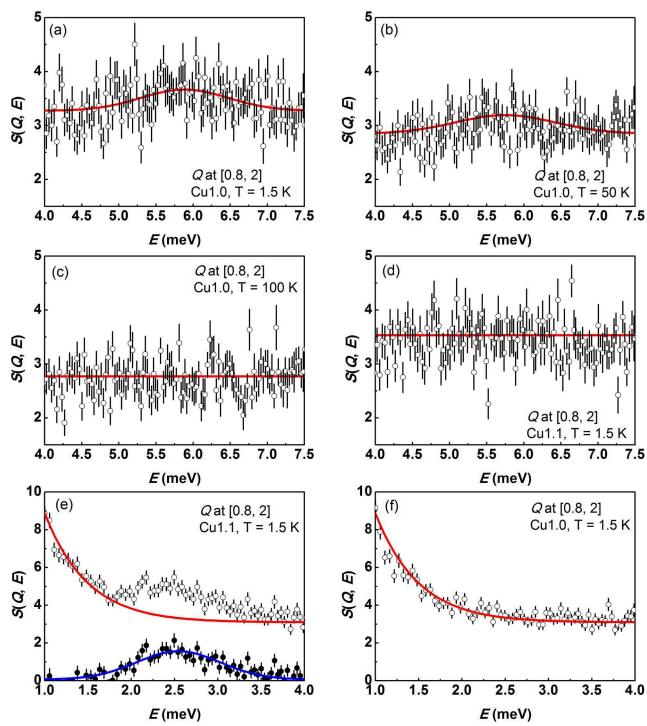


Figure 6

29Dec2015

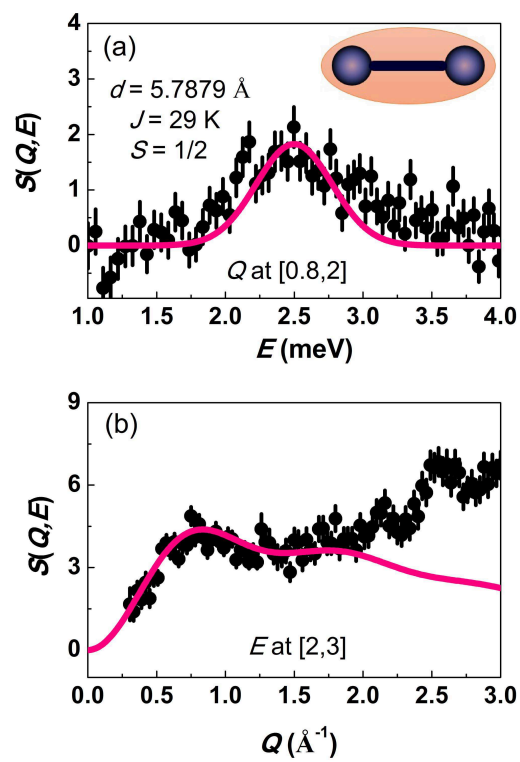


Figure 7

29Dec2015